Journal of Solid State Chemistry 184 (2011) 1216–1220

Contents lists available at ScienceDirect

Journal of Solid State Chemistry

journal homepage: www.elsevier.com/locate/jssc

Thermally stimulated crystallization of $(20-x)LiO_2$–$80TeO_2$–xWO_3 glass system

S.M. Sidel, W.A. Capanema Jr., E.B. Araujo, J.C.S. Moraes *, K. Yukimitu

Faculdade de Engenharia, UNESP—Univ Estadual Paulista, Ilha Solteira, SP, Brazil

ARTICLE INFO

Article history:
Received 11 November 2010
Received in revised form
4 March 2011
Accepted 5 March 2011
Available online 15 March 2011

Keywords:
Glasses
Tellurium
Crystallization
Activation energy

ABSTRACT

Tellurite glasses of the $(20-x)LiO_2$–$80TeO_2$–xWO_3 system were synthesized ($x=0$, 5, and 10) and annealed at different temperatures, and the crystallization kinetics was studied using XRD, FTIR spectroscopy, and DSC techniques. XRD data evidenced the amorphous state of *as-quenched* samples, while thermally treated samples showed the growth of crystalline phases. FTIR spectroscopy was used to observe the evolution of the vibrational mode assigned to the TeO_2 phases. The presence of γ-TeO_2, α-TeO_2, and α-$Li_2Te_2O_5$ crystalline phases was observed for the sample TL, $x=0$, while only the first and second phases were observed for TLW5 and TLW10 samples, $x=5$ and 10, respectively, suggesting that WO_3 enters the structure preferentially as glass former, inhibiting the growth of the phase α-$Li_2Te_2O_5$.

1. Introduction

The development of lasers, and their use in telecommunication systems, has stimulated the research and development of new glass systems. Glasses based on tellurium oxide (TeO_2) are of scientific and technological interest because of their interesting properties: low melting temperature, high refractive indices, high third order nonlinear susceptibility, and low phonon energy. Such properties make telluride glasses promising for use in amplifiers and nonlinear optical devices [1–6]. Among different studies on glasses, there are those devoted to manufacturing of nanostructured transparent glass-ceramics, which show the second harmonic generation [7,8]. Other studies show that the intensity of fluorescence frequency up-conversion for Er^{3+}-doped tellurium glass–ceramics has a high increase, when compared to its precursor telluride glass [9,10]. Thus, the development of TeO_2-based glass-ceramics as functional optical material requires control and knowledge of the thermally assisted nucleation and crystallization process into the glass bulk. In order to understand these processes, it is important to investigate the evolution of the crystalline phases in the amorphous structure and to understand the effects of this transformation on the physical properties of the glasses. For this reason, Imaoka and Yamazaki [11] examined the glass-forming regions in various TeO_2-based systems. They observed that the systems of R_2O–WO_3–TeO_2 (R=Li, Na, K) have wide glass-forming regions, which make them suitable for studies on thermal stability, crystallization behavior, and structural relaxation of glasses based on TeO_2. Kosuge et al. [12] investigated the thermal stability and heat capacity changes in the glass transition region of K_2O–WO_3–TeO_2 glasses to examine the structural relaxation behavior. This study showed that TeO_2-based glasses present interesting thermal features. For example, the glass $15K_2O$–$15WO_3$–$70TeO_2$ shows large heat capacity changes and high thermal stability against crystallization, in the glass transition region.

Recently, the authors of the current study reported the results from a study of the effects of particle size and nucleation temperature on tellurite $20Li_2O$–$80TeO_2$ glass crystallization [13]. The results suggested a crystallization order on the glass matrix of the γ-TeO_2, α-TeO_2, and $Li_2Te_2O_5$ phases.

To continue earlier works, the purpose of this work was to study the crystallization process on the structural and thermal properties of the xWO_3–$(20-x)Li_2O$–$80TeO_2$ glass system. The experimental techniques used were powder X-ray diffraction (XRD), Fourier transform infrared spectroscopy (FTIR), and differential scanning calorimetry (DSC).

2. Experimental procedure

The tellurite glasses were prepared by the conventional method of melt-quenching from the following analytical grade reagents: lithium carbonate, Li_2CO_3 (Sigma-Aldrich, 99+%); tellurium oxide, TeO_2 (Sigma-Aldrich, 99+%); and tungsten oxide, WO_3 (Sigma-Aldrich, 99+%). Three samples were prepared with

* Correspondence to: Departamento de Física e Química—UNESP, Av. Brasil 56, 15.385-000 Ilha Solteira, São Paulo, Brazil. Fax: +55 18 3742 4868.
E-mail address: joca@dfq.feis.unesp.br (J.C.S. Moraes).

0022-4596/$ - see front matter © 2011 Elsevier Inc. All rights reserved.
doi:10.1016/j.jssc.2011.03.013

the following compositions: $20Li_2O–80TeO_2$, $15Li_2O–80TeO_2–5WO_3$, and $10Li_2O–80TeO_2–10WO_3$. These samples will be referred to, henceforth, as TL, TLW5, and TLW10, respectively.

Appropriate amounts of the reagents mixture were first calcined for CO_2 liberation and then melted into the platinum crucible using an electric furnace set at the following melting temperatures: 1023 K for TL, and 1123 K for TLW5 and TLW10. The samples were fused for 30 min. The molten material was poured into a brass mold for quenching, and annealed for 2 h, at 473 K for TL, and 523 K for TLW5 and TLW10, to relieve the mechanical tensions. The obtained glass samples present a transparent greenish yellow color.

The analysis of the glass structure was accomplished by the XRD technique, using a Rigaku Rotaflex RU200B diffractometer with CuK anode. The FTIR spectra were obtained in transmission mode from powdered samples dispersed in tablets of KBr using a Nicolet Nexus 670 spectrometer. The spectra were recorded at room temperature, in the 1200–400 cm^{-1} range.

Thermal parameters [14–16] were determined by the DSC technique using TA Instruments' DSC 2920 (temperature accuracy of ± 0.1 K) and a 10 mg samples of powdered glass contained in an aluminum pan with dry nitrogen streaming through the heating chamber. The samples were submitted to different heating rates (2.5, 5.0, 7.5, 10.0, and 12.5 K min^{-1}).

3. Results and discussion

Samples with particle sizes of 45–63 μm were thermally treated at different temperatures in an electric furnace for 5 min. The thermal treatment temperatures were chosen between glass (T_g) and crystallization (T_x) temperatures based on DSC data.

Fig. 1 shows XRD patterns of the TL *as-quenched* glass (I) and glasses treated at 548 (II), 597 (III), 608 (IV), and 634 K (V). Curves I, II, and III show the typical characteristics of amorphous materials. On the other hand, the samples treated at 608 and 634 K exhibit a diffraction pattern typical of glass-ceramic, as illustrated in curves IV and V, respectively. The indexed peaks in these curves were ascribed to the α-TeO_2 (paratellurite), γ-TeO_2, and α-$Li_2Te_2O_5$ crystalline phases [13,17]. The α-TeO_2 and γ-TeO_2 crystalline phases are polymorph phases of tellurium oxide (TeO_2), where the γ phase is considered a metastable structure [18,19]. Both structures are essentially built up from similar basic TeO_4 units interconnected in the same way—via the $Te–_{eq}O_{ax}–Te$ simple bridges [19–21]. The difference between them is the existence of two types of Te–O–Te bridges in γ-TeO_2, less symmetric and much more symmetric than the bridges in α-TeO_2 [19]. Although on pure TeO_2 glass the first crystalline phase to appear is the γ-TeO_2 [20], it is impossible to know, based on the diffraction patterns of Fig. 1, whether α-TeO_2, γ-TeO_2, and α-$Li_2Te_2O_5$ phases crystallize simultaneously or at distinct onset crystallization temperatures. However, the results obtained in our previous work indicate that the crystallization of the $Li_2Te_2O_5$ phase occurs after the α- and γ-TeO_2 phases [13].

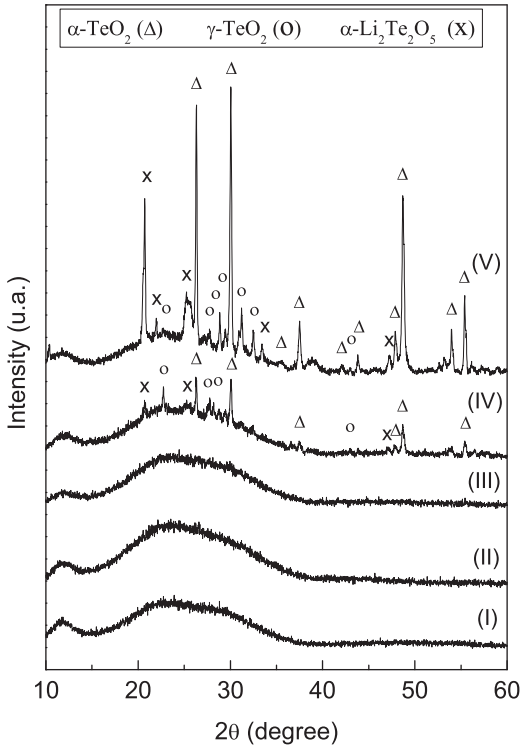

Fig. 1. XRD diffractogram of the TL glass: (I) *as-prepared*, treated at 548 (II), 597 (III), 608 (IV), and 634 K (V) for 45–63 μm grain size.

XRD data were obtained for the TLW5 (Fig. 2A) and TLW10 (Fig. 2B) glasses in a similar way. In Fig. 2A, the diffraction patterns I, II, and III refer to the TLW5 *as-quenched* glass and the TLW5 glass treated at 553 and 643 K, respectively. These three diffraction patterns present characteristics of an amorphous material, while diffraction pattern IV of the glass treated at 653 K exhibits the presence of α-TeO_2 and γ-TeO_2 crystalline phases. On the other hand, the diffraction pattern of glass treated at 663 K (V) presents only the α-TeO_2 phase, indicating that the γ-lattice appears in the first crystalline phase, as observed on the pure TeO_2 glass [18–20,22].

Fig. 2B shows the diffraction patterns obtained for TLW10 samples. The characteristics of an amorphous material were observed in the diffraction patterns of the *as-quenched* glass (I) and of the treated glass at 658 K (II). The diffraction patterns of the samples treated at 681 (III) and 689 K (IV) exhibit the presence of the α-TeO_2 and γ-TeO_2 phases. As observed in the TLW5 glass, the γ-TeO_2 phase disappeared completely when the TLW10 glass was treated at 713 K, exhibiting only the diffraction peaks of the α-TeO_2 phase.

The XRD patterns obtained for TLW5 and TLW10 glasses did not show the crystallization of any phase due to the addition of WO_3, indicating that the tungsten remains into the amorphous glass phase. The WO_3 crystalline phase has been observed in tungsten tellurite glasses with the WO_3 content ≥ 15 mol% [22].

The XRD study of the glasses was complemented with FTIR spectroscopy. Fig. 3 shows the spectra of the TL *as-quenched* glass (I) and glasses treated at 548 (II), 597 (III), 608 (IV), and 634 K (V). Spectra I, II, and III show a major band at around 607 and the shoulder at 775 cm^{-1}, which are, respectively, assigned to vibrations of Te–O–Te bridges between two TeO_4 trigonal bipyramids (btp) and vibrations of Te=O bonds of TeO_3 trigonal pyramids (tp) [23,24]. These three spectra exhibit the typical broadening of the vibration bands due to the glassy state [23], indicating that significant structural change did not occur when the *as-quenched* glass was treated at 548 and 597 K. On the other hand, significant changes are observed in spectra IV and V. The sample treated at 634 K (V) presents absorption bands at 453, 576, 677, and 775 cm^{-1}. The infrared spectrum of the α-TeO_2 is characterized by two pronounced absorption bands at around 660 and 770 cm^{-1} [20,23], and the infrared spectrum of the γ–TeO_2 exhibits two absorption bands at around 440 and 660 cm^{-1} [20]. Therefore, the presence of 453, 677, and 775 cm^{-1} absorption bands in spectra V attests the crystallization of the α-TeO_2 and γ-TeO_2 phases. This conclusion is in good agreement with the XRD results (Fig. 1-V). The absorption band observed at 607 cm^{-1} in the *as*-quenched glass (I) shifted to 576 cm^{-1} with the thermal treatment.

Fig. 4A and B illustrate the infrared spectra of the TLW5 and TLW10 glasses, respectively, *as-quenched* and thermally treated.

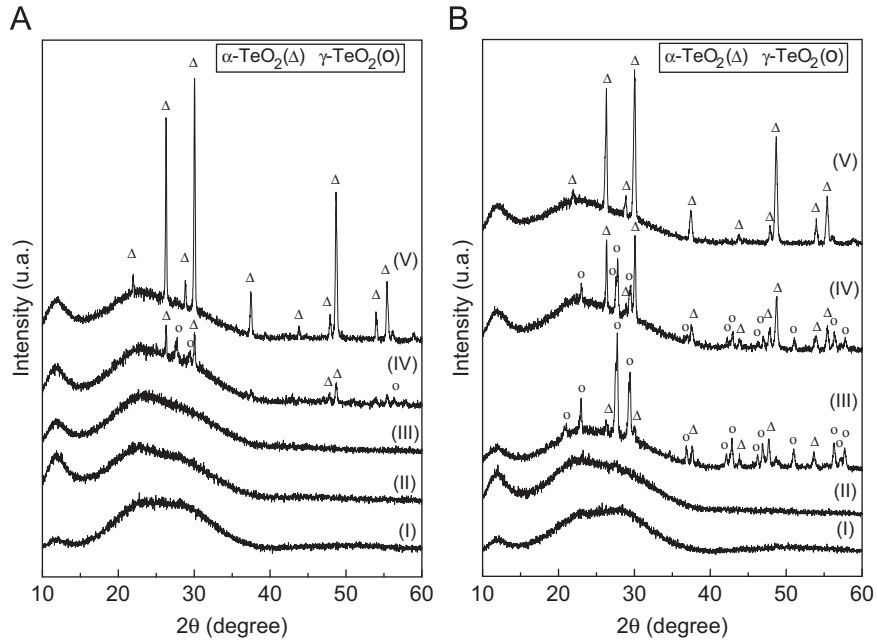

Fig. 2. XRD diffractogram of glasses: (A) TLW5 *as-quenched* (I) and treated at 553 (II), 643 (III), 653 (IV), and 663 K (V); (B) TLW10 *as-quenched* (I); treated at 658 (II), 681 (III), 689 (IV), and 713 K (V) for 45–63 μm grain size.

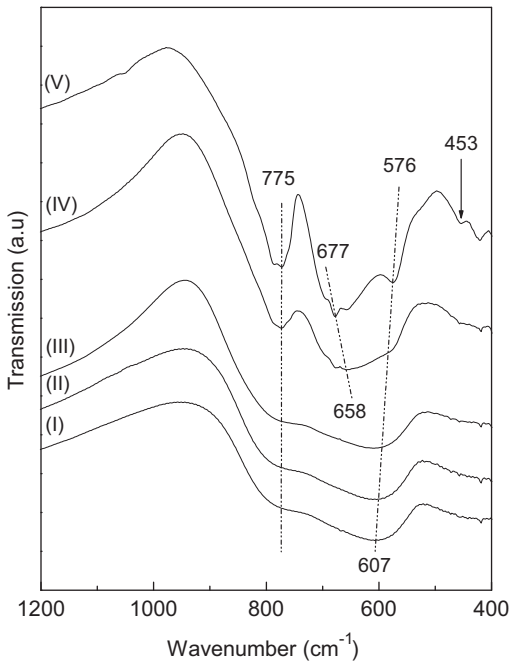

Fig. 3. Infrared transmission spectra of TL glass: (I) *as-quenched* and treated at 548 (II), 597 (III), 608 (IV), and 634 K (V) for grain size < 38 μm.

Both glasses present similar absorption peaks except for the TLW10 glass treated at 681 and 689 K, which shows an absorption peak at 440 cm^{-1}. No significant change was observed when the TLW5 *as-quenched* glass was treated at 553 (Fig. 4A-II) and 643 K (Fig. 4A-III). The shift (from 613 to 585 cm^{-1}) of the absorption peak ascribed to TeO_4 btp and the definition of the absorption band of the α-TeO_2 phase at around 660 cm^{-1} were observed only with the thermal treatment at 653 (Fig. 4A-IV) and 663 K (Fig. 4A-V). For TLW10 glass, these changes occurred only when the *as-quenched* glass was treated at 681 (Fig. 4B-III), 689 (Fig. 4B-IV), and 713 K (Fig. 4B-V). Furthermore, the absorption peak characteristic of the γ-TeO_2 phase, located at 440 cm^{-1}, appeared when the *as-quenched* sample was treated at 681 and 689 K but it is not present in the sample treated at 713 K. This feature was also observed in the XRD data (Fig. 2B). Finally, the absorption band at 855 and 920 cm^{-1} for TLW5, and 855 and 925 cm^{-1} for TLW10, are ascribed to vibration of the W−O bond [23,25].

Fig. 5 shows the DSC curves of TL (I), TLW5 (II), and TLW10 (III) glasses at different heating rates (Φ). It can be observed that adding WO_3 to the glass composition induces an increase in the temperatures of glass transition (T_g) and maximum crystallization (T_x). The observed asymmetry of crystallization peaks suggests an overlapping of distinct crystallization phases, as previously observed in XRD results.

Table 1 summarizes the thermal parameters obtained from the DSC curve corresponding to the heating rate of $\Phi = 2.5$ K min^{-1}. T_g and T_x move toward high temperatures with the addition of WO_3, pointing out that tungsten enters as glass former. The temperature values of the three crystallization peaks for TL glass and the two for TLW5 and TLW10 glasses were determined from deconvolution of DSC peaks using the Gaussian function.

The activation energy of crystallization (E) was determined using Kissinger's [14] relation: $\ln(T_p/\phi) = E/RT_p + \text{constant}$, where T_p is the temperature corresponding to the maximum of the DSC crystallization curve, ϕ is the heating rate, and R is the gas constant. E is obtained directly from the slope of the $\ln(T_p^2/\phi) \times 1/T_p$ plot (Fig. 6). According to Fig. 1, the first crystalline phase to appear in the TL glass is γ-TeO_2, followed by α-TeO_2, and then by α-$Li_2Te_2O_5$. This sequence [17] is in agreement with the E_1, E_2, and E_3 activation energy values shown in Table 1.

4. Conclusions

The thermally stimulated crystallization of the TL, TLW5, and TLW10 glasses was investigated as a function of the thermal treatment temperature. The XRD and FTIR results revealed that the crystalline phases observed in TL glass were γ-TeO_2, α-TeO_2, and α-$Li_2Te_2O_5$, and that WO_3 in the glass matrix inhibits the

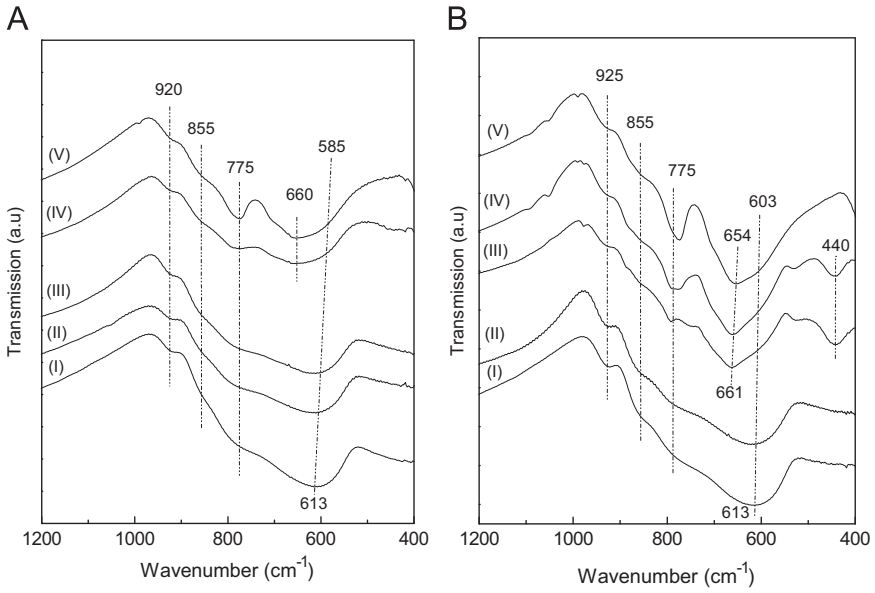

Fig. 4. Infrared transmission spectra of glasses: (A) TLW5 *as-quenched* (I) and treated at 553 (II), 643 (III), 653 (IV), and 663 (V); (B) TLW10 *as-quenched* (I) and treated at 658 (II), 681 (III), 689 (IV), and 713 K (V) for grain size < 38 μm.

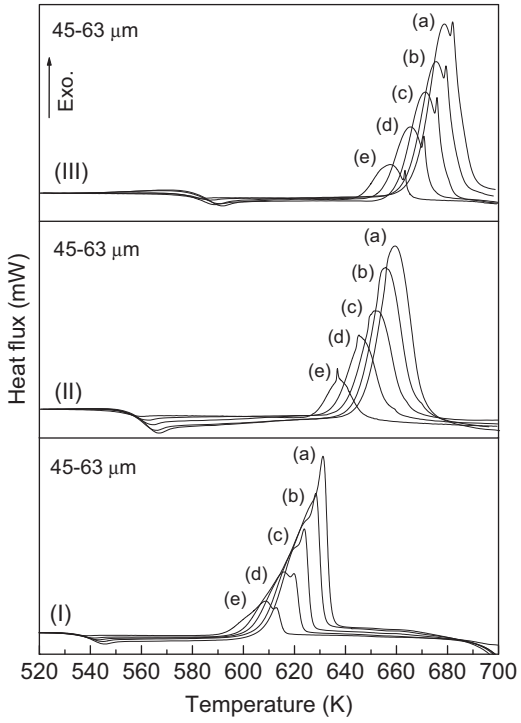

Fig. 5. DSC thermogram for glasses: (I) TL, (II) TLW5, and (III) TLW10 for different heating rates (ϕ): (a) 12.5, (b) 10.0, (c) 7.5, (d) 5.0, and (e) 2.5 K min^{-1} for 45–63 μm grain sizes. Insert graphic shows as the T_g is evaluated.

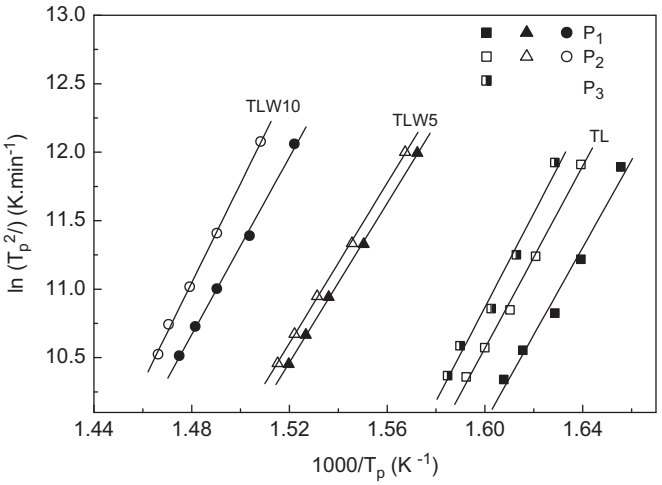

Fig. 6. $\ln(T_p^2/\phi)$ *versus* $(1000/T_p)$ for TL, TLW5, and TLW10 glasses for crystallization peak temperature showed in the Table 1.

Table 1
Thermal parameters of the TL, TLW5, and TLW10 glasses for 45–63 μm grain size and heating rate of 2.5 K min^{-1}.

Samples	T_g (K)	T_x (K)	Peak temperature (K)			Energies (kJ mol^{-1})		
			T_{p1}	T_{p2}	T_{p3}	E_1	E_2	E_3
TL	526	584	604	610	614	265 ± 9	276 ± 5	285 ± 8
TLW5	548	621	636	638	–	242 ± 1	243 ± 1	–
TLW10	570	639	657	663	–	269 ± 3	302 ± 3	–

formation of the α-$Li_2Te_2O_5$ phase. From XRD and FTIR data, it was possible to observe that the γ-TeO_2 phase crystallized before the α-TeO_2 phase, as observed in the pure TeO_2 glass. DSC data showed that increasing WO_3 in the glass composition increases the T_g and T_x temperatures. Furthermore, the results suggest that WO_3 enters the structure as glass former and does not participate in the crystallization of glass.

Acknowledgments

The authors thank the CAPES, CNPq, and FAPESP Brazilian research agencies for the financial support.

References

[1] A.K. Yakhkind, J. Am. Ceram. Soc. 49 (1966) 670.
[2] H. Nasu, O. Matsushita, K. Kamiya, K. Kubodera, J. Non-Cryst. Solids 124 (1990) 275–277.

[3] S.H. Kim, T. Yoko, S. Sakka, J. Am. Ceram. Soc. 76 (1993) 2486–2490.
[4] S.H. Kim, T. Yoko., J. Am. Ceram. Soc. 78 (1995) 1061–1065.
[5] J. Hecht, Opt. Photonics News 13 (2002) 36–39.
[6] S.A. Cerqueira, Rep. Prog. Phys 73 (2010) 1–21.
[7] F. Torres, Y. Benino, T. Komatsu, J. Mater. Sci. 36 (2001) 4961–4967.
[8] E.D. Jeong, P.H. Borse, J.S. Lee, M.G. Ha, H.K. Park, T. Komatsu, H.G. Kim, J. Ind. Eng. Chem. 12 (2006) 790–794.
[9] K. Hirano, Y. Benino, T. Komatsu, J. Phys. Chem. Solids 62 (2001) 2075–2082.
[10] C. Yu, J. Zhang, L. Wen, Z. Jiang, Mater. Lett. 61 (2007) 3644–3646.
[11] M. Imaoka, T. Yamazaki, J. Ceram. Soc. Jpn 76 (1968) 160–172.
[12] T. Kosuge, Y. Benino, V. Dimitrov, R. Sato, T. Komatsu, J. Non-Cryst. Solids 242 (1998) 154–164.
[13] E. Idalgo, E.B. Araújo, K. Yukimitu, J.C.S. Moraes, V.C.S. Reynoso, C.L. Carvalho, Mat. Sci. Eng. A: Struct. 434 (2006) 13–18.
[14] H.E. Kissinger, J. Res. Nat. Bur. Stand. 57 (1956) 217–221.
[15] K. Cheng, Mat. Sci. Eng. B: Solid (1999) 194–199.
[16] E.D. Zanoto, A. Gualhardi, J. Non-Cryst. Solids 104 (1988) 73–80.
[17] E.B. Araújo, E. Idalgo, A.P.A. Moraes, A.G. Souza Filho, J. Mendes Filho, Mater. Res. Bull. 44 (2009) 1596–1600.
[18] P.A. Thomas, J. Phys. C: Solid State 21 (1988) 4611–4627.
[19] J.C. Champarnaud-Mesjard, S. Blanchandin, P. Thomas, A. Mirgorodsky, T. Merle-Mejean, B. Frit, J. Phys. Chem. Solids 61 (2000) 1499–1507.
[20] O. Nogueira, T. Merle-Mejean, A.P. Mirgorodsky, M.B. Smirnov, P. Thomas, J.C. Champarnaud-Mesjard, J. Non-Cryst. Solids 330 (2003) 50–60.
[21] O. Lindqvist, Acta Chem. Scand. 22 (1968) 977–982.
[22] S. Blanchandin, P. Marchet, P. Thomas, J.C. Champarnaud-Mesjard, B. Frit, A. Chagraoui, J. Mater. Sci. 34 (1999) 4285–4292.
[23] P. Charton, L. Gengembre, P. Armand, J. Solid State Chem. 168 (2002) 175–183.
[24] V.O. Sokolov, V.G. Plotnichenko, V.V. Koltashev, E.M. Dianov, J. Non-Cryst. Solids 352 (2006) 5618–5632.
[25] I. Shaltout, Y. Tang, R. Rraunstein, E.E. Shaisha, J. Phys. Chem. Solids 57 (1996) 1223–1230.